

SUPA: A Lightweight Diagnostic Simulator for Machine Learning in Particle Physics

Atul Kumar Sinha^{*1} Daniele Paliotta^{*1} Bálint Máté^{*1} Sebastian Pina-Otey¹ John A. Raine¹
Tobias Golling¹ François Fleuret¹

Abstract

Deep learning methods have gained popularity in high energy physics for fast modeling of particle showers in detectors. Detailed simulation frameworks such as the gold standard GEANT4 are computationally intensive, and current deep generative architectures work on discretized, lower resolution versions of the detailed simulation. The development of models that work at higher spatial resolutions is currently hindered by the complexity of the full simulation data, and by the lack of simpler, more interpretable benchmarks.

Our contribution is SUPA, the SUrrogate PARTicle propagation simulator, an algorithm and software package for generating data by simulating simplified particle propagation, scattering and shower development in matter. The generation is extremely fast and easy to use compared to GEANT4, but still exhibits the key characteristics and challenges of the detailed simulation. We support this claim experimentally by showing that performance of generative models on data from our simulator reflects the performance on a dataset generated with GEANT4. The proposed simulator generates thousands of particle showers per second on a desktop machine, a speed up of up to 6 orders of magnitudes over GEANT4, and stores detailed geometric information about the shower propagation. SUPA provides much greater flexibility for setting initial conditions and defining multiple benchmarks for the development of models. Moreover, interpreting particle showers as point clouds creates a connection to geometric machine learning and provides challenging and fundamentally new datasets for the field.

The code for SUPA is available at <https://github.com/itsdaniele/SUPA>.

^{*}Equal contribution ¹University of Geneva, Switzerland. Correspondence to: Atul Kumar Sinha <atul.sinha@unige.ch>.

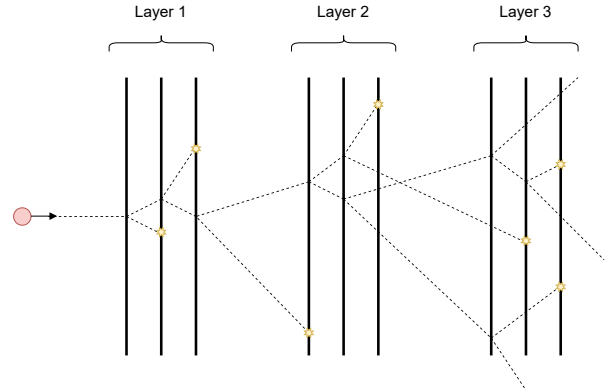


Figure 1: Schematic summary of a propagation event generated by SUPA. Splitting events can happen at the black vertical lines, called *slices*. See § 3 and Figure 3 for a detailed explanation of the process.

1. Introduction

In order to understand the fundamental building blocks of nature, High Energy Physics (HEP) experiments involve highly energetic particle collisions. These collisions cause particles to decay, and the identification of the resulting decay particles is of key importance to develop and confirm new physics/theories. This is enabled through an electromagnetic or hadronic calorimeter. As particles interact with the calorimeter, they split into multiple other particles, forming a particle shower. The nature of the generated shower depends on the specific material and geometry of the calorimeter, which are carefully selected and driven by physics theory and practical considerations. The generated shower deposits energy in active layers of the calorimeters, and provides energy and location measurements from the particles produced in the cascade.

Precise computer simulation is central to a better understanding of experimental results in HEP. Simulation is especially useful for the task of event reconstruction, where the deposited energy in the calorimeter is used to identify the particle that originated a given shower. The pattern of the

deposited energy depends on the specific type of the (intermediate) particles, the initial energy and incidence angle, as well as the specific geometry and shape of the detector material, among other factors. The state-of-the-art for this kind of simulations is GEANT4 (Agostinelli et al., 2003), a Monte Carlo toolkit for modeling the propagation of particles through matter.

While detailed simulation through GEANT4 provides fine-grained shower generation and captures the underlying distributions accurately, this software consists of more than 3.5 millions lines of C++, is computationally very expensive, and requires specific domain knowledge to be set up and tuned. This makes it cumbersome and expensive to produce the amount and diversity of data needed to speed up machine learning research on these topics.

Our key contributions to ease these issues are:

- We introduce SUPA: a fast, easy to use simulator for simple particle propagation, scattering and shower development in matter (see § 3).
- We experimentally demonstrate that SUPA can be used as a proxy for detailed simulation, while being easy to tune and up to 6 orders of magnitude faster than GEANT4 (see § 5.1).
- We use SUPA to generate data that highlights the limitations of current machine learning approaches for fast shower simulation (see § 5.2).

1.1. Image Representation

Existing approaches for generating particle showers (Paganini et al., 2018a; Krause & Shih, 2021) focus on a quantized representation of the calorimeter hits, binning them into discrete pixels, or cells, and setting the pixel intensity to the sum of the energy deposited. The upside of this approach is that, due to the structure of existing calorimeters, the data takes the form of low resolution images and standard computer vision models can be directly applied. However, as we increase the resolution of the quantized representations in order to preserve more information, the resulting images become exceedingly sparse, leading to difficulties in training existing machine learning architectures.

It is also important to notice that, when decreasing the resolution of the data and looking at showers, while the signal to model is of lower dimension and less sparse, the underlying structure and relationships between hits are lost. This requires models to implicitly learn equivariations from multiple examples, while also introducing artificial structure arising from the chosen detector geometry. For example, with a shower incident on the surface of a detector, a slight translation in either direction does not change the properties of the shower. However it still has an impact on the resulting

datasets, where for small shifts it is not translationally equivariant. Having access to the underlying energy depositions would therefore present a solution to geometry dependence in the models, and allow generative models to learn the underlying structure from the physical process directly.

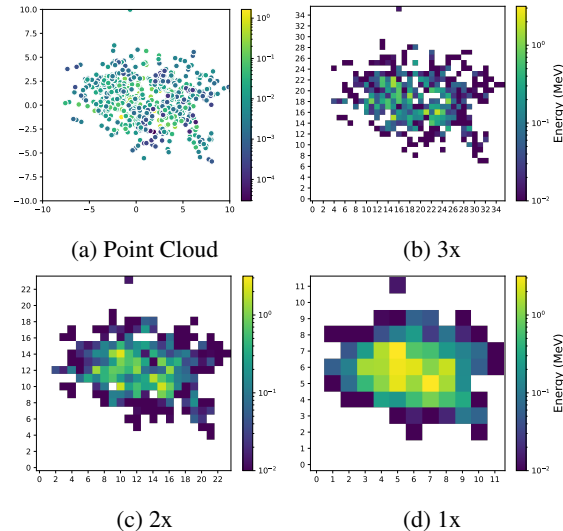


Figure 2: An example shower (single layer) shown at different resolutions

1.2. Point Cloud Representation

Many popular point-cloud datasets (Wu et al., 2015; Chang et al., 2015) in the machine learning community contain shape representations of physical objects, such as points sampled uniformly from the surfaces of chairs, tables, etc. These datasets enjoy many nice properties, e.g. locality and redundancy, that calorimetry datasets do not. Moreover, existing generative models for point clouds rely on these simplifying assumptions and therefore performance of more diverse datasets is still relatively unexplored. In the case of particle showers in calorimeters, dealing directly with the point cloud representation provides an optimal description of the underlying physics processes. However, due to the detailed simulation resulting from GEANT4, the number of points per shower represents a huge computational challenge.

A key objective of our synthetic simulator is to bridge this gap by allowing for quicker ground truth data generation for different initial settings, thus providing a way of modulating the complexity of the dataset, leading to more interpretable benchmarks.

2. Related Work

Shower simulation with GEANT4 requires a complete description of the geometry and material of the detector and

simulates all interactions between the initial particle, any subsequently produced particles through decays or emissions, and the detector material. The upside of using GEANT4 for simulation is that it is very accurate and represents the underlying physical phenomena precisely, but it comes at the cost of being computationally very expensive. Moreover, it requires expertise to define the configuration and a multitude of expert hours to set it up for new detector geometries. To reduce the computational resources required to simulate particle physics collisions and their energy depositions in detectors, deep generative models have been applied to generate particle showers. Most of these models (Abhishek et al., 2021; Krause & Shih, 2021; Paganini et al., 2018b) employ the dataset first introduced in CaloGAN (Paganini et al., 2018b) which is based on a simplified calorimeter inspired by the ATLAS Liquid Argon (LAr) electromagnetic calorimeter.¹

2.1. Datasets and calorimeter structure

For the CaloGAN dataset, the calorimeter is cubic in shape with each dimension being 480 mm and no material in front of it. The volume is divided into three layers along the radial (z) direction with varying thicknesses of 90 mm, 347 mm, and 43 mm, respectively. These layers are further segmented into discrete cells, with different sizes for each layer: 160 mm \times 5 mm (first layer), 40 mm \times 40 mm (second layer) and 40 mm \times 80 mm (third layer). Each layer can be represented as a single-channel two-dimensional image with pixel intensities representing the energy deposited in the region. The final read-out has the resolution of 3 \times 96, 12 \times 12, and 12 \times 6. For this dataset, three different particle types were considered, namely, positrons, charged pions and photons. Further, the particles were configured to be incident perpendicular to the calorimeter with initial energies uniformly distributed in the range between 1 GeV and 100 GeV.

Several other calorimeter geometries and configurations are employed across the literature. Erdmann et al. (2019) consider a calorimeter configuration motivated by the CMS High Granularity Calorimeter (HGCAL) prototype, while Belayneh et al. (2020) study a calorimeter based on the geometric layout of the proposed Linear Collider Detector (LCD) for the CLIC accelerator. (Buhmann et al., 2021b;a) investigate the prototype calorimeter for the International Large Detector (ILD) which is one of the two proposed detector concepts for the International Linear Collider (ILC). In a different application setting, Erdmann et al. (2018) model a calorimeter response for cosmic ray-induced air showers in the Earth’s atmosphere, producing signals in

¹The ATLAS calorimeter has e.g. a more complex geometry, with the cells having accordion shaped electrodes to maximise the active volume

ground based detector stations. In contrast to the CaloGAN calorimeter, it has a single readout layer with 9 \times 9 cells, each cell corresponds to a detector unit placed with a spacing of 1500 m. Although many different detector technologies are considered in the various models, the common aspect between the models and the corresponding datasets is the projection of the spatial signal onto discretized cells in 2D planes or a generalized 3D volume. The projection is done either directly while designing the calorimeter geometry, or as a post processing step. Further, the number of cells and thus the resolution of the final read-out is usually kept small. This is done either to simplify the data for training the models, or in order to speed up the simulations.

Due to the different geometries used for generating the datasets, it is not a straightforward task to compare the performance of the various models. As the developments of each shower are completely dependent on the detailed model of the detector in GEANT4, although the same initial particles can be simulated, it is very difficult to draw parallels between two different datasets, as it is not possible simply to change the representation of the data from one model to look like that of another.

2.2. Deep Generative Models

The applications of deep generative modeling to calorimeter simulation have so far almost entirely focused on Generative Adversarial Networks (GANs, Goodfellow et al. 2014) and Normalizing Flows (Rezende & Mohamed, 2016). CaloGAN (Paganini et al., 2018a) was the first application of GANs to a longitudinally segmented calorimeter. The approach is based on LAGAN (de Oliveira et al., 2017), a DCGAN (Radford et al., 2016)-like architecture, that is able to synthesize the shower images. The generator outputs a gray-scale image for each layer in the calorimeter, with each output pixel representing the energy pattern collected at that location. The architecture is also complemented with an auxiliary classifier tasked with reconstructing the initial energy E .

Krause & Shih (2021) improve on CaloGAN with CaloFlow, a normalizing flow architecture to generate shower images. CaloFlow is able to generate better samples than previous approaches based on GANs and VAEs, while also providing more stable training.

Previous work by the ATLAS collaboration (2018) proposes to use a Variational Autoencoder (Kingma & Welling, 2014) on the flattened images. Both the encoder and decoder consist of an MLP conditioned on the energy of the initial particle. In addition to the reconstruction and KL-terms, the authors also optimize for the overall energy deposit in both in the individual layers and in the overall system.

3. Propagation Model

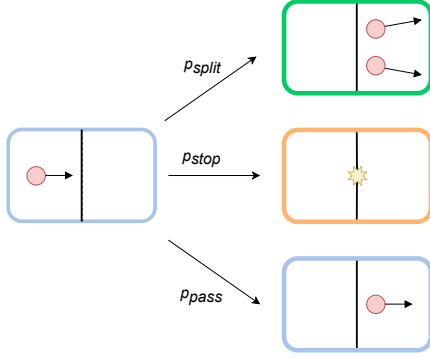


Figure 3: Schematic view of SUPA’s propagation model. Each time a particle crosses a pre-defined “slice”, it either splits in two, stops and deposits energy, or passes through unperturbed.

SUPA generates data that imitates the propagation and splitting/scattering of point particles. To generate an event, a point particle is initialized at the origin of the 3D space with an initial energy² value and a velocity parallel to the z -axis. We then define a sequence of 2D planes orthogonal to the z -axis at $\{z_0, \dots, z_N\}$ that we call “slices.” As the initial particle reaches the first predefined z -slice at z_0 , it has 3 options (see Figure 3): stop and deposit its energy with probability p_{stop} , split into two with probability p_{split} , or simply continue moving with the same velocity with probability $p_{\text{pass}} = 1 - (p_{\text{stop}} + p_{\text{split}})$. Then:

- If the particle splits, two particles are generated at the splitting location with energy and velocity features that ensure momentum conservation, i.e., that the sum of momentum vectors of the new particles is equal to the decaying one. The original particle is removed from the propagation model and the two new ones continue propagating with their respective velocities.
- If the particle stops, its energy is deposited and the energy value and the location of the hit are recorded.
- If the particle passes, it simply continues with its original velocity.

See Algorithm 1 for the pseudocode of this process. We can think of it as detector layer being positioned at the z_0 -slice recording energy deposits. After the slice at z_0 , the model either contains 0, 1 or 2 particles still propagating.

²A continuous attribute obeying simple conservation laws at each splitting, which can be interpreted as an equivalent for the energy of the particles in a shower. As such, we refer to this property as the energy.

As they reach the additional slices at $\{z_1, \dots, z_N\}$ the above procedure is repeated: whenever a particle is at a z -slice, it either passes, deposits its energy or decays.

After all particles crossed the last slice at z_N we collect all energy deposits (energy value and 3D location). Instead of building a dataset from the exact 3D location of these deposits, we partition the slices into subsets we call layers L_i :

$$\begin{aligned} L_1 &= \{z_0, \dots, z_{i_1}\}, \\ L_2 &= \{z_{i_1+1}, \dots, z_{i_2}\}, \\ &\dots \\ L_n &= \{z_{i_{n-1}+1}, \dots, z_N\}, \end{aligned}$$

and build an event from the energy deposit E and the (x, y) -coordinate of all hits for all slices within a given layer L_i , effectively projecting the z -axis into a single point. An event then consists of N 2D point clouds, one for each layer, with a single scalar feature per point. Intuitively, the slices z_i are the positions where the particle can split and stop (granularity of the simulation), and the layers L_i correspond to the detector layers, where the readout happens. Figure 1 contains a schematic summary for the propagation process.

Having complete control over the algorithm, we can increase/decrease the complexity of the generated data by adjusting the distribution of the properties of the initial particle, the number and location of the slices z_i , the probabilities $p_{\text{stop}}, p_{\text{pass}}, p_{\text{split}}$ and the distribution of the properties of the children after a splitting event. This is especially useful to debug and understand the behaviour of machine learning models at different levels for complexity.

Downsampling. We downsample the point clouds to their corresponding image representation (see Figure 2) by first defining the region of interest i.e. a rectangular region for each layer and the number of bins/cells/pixels in both the horizontal (or η) and vertical (or ϕ) directions. Finally, for each cell, we sum the energy of all the points falling within it to get the pixel intensity. We can increase the number of cells in order to get higher resolutions. Figure 2b, 2c, and 2d show the downsampled image representations at resolutions of 3x, 2x and 1x respectively for the shower shown in Figure 2a. We choose 1x to be the same resolution as used in CaloGAN (Paganini et al., 2018a) (i.e. 12×12 for Layer 1).

Notation. We denote a single shower as $\mathbf{x} = \{\mathbf{x}_{L_1}, \mathbf{x}_{L_2}, \dots, \mathbf{x}_{L_N}\}$, where \mathbf{x}_{L_i} denotes the i^{th} layer and N is the total number of layers considered. For the point cloud representation, \mathbf{x}_{L_i} can be further expanded as $\mathbf{x}_{L_i} = \{\mathbf{x}_1^i, \mathbf{x}_2^i, \dots, \mathbf{x}_{N_i}^i\}$, where N_i denotes the total number of points in layer i of the shower (can vary across showers). Further, each point is a vector $\mathbf{x}_j^i = [\eta_j^i, \phi_j^i, E_j^i]$, where η and ϕ are the coordinates and E denotes the energy. For the

Table 1: Comparison of GEANT4 and the proposed model (SUPA)

	GEANT4	SUPA
codebase	3.6m lines in C++	few hundred lines in Python
target usage	detailed physics simulations	fast data generation
speed	1772 ms/shower [†]	100 ms/shower [‡]

[†]The exact simulation time depends on the incident particle and its kinematic properties, as well as the detailed composition of the detector geometry in the GEANT4 model. These numbers are taken for the CaloGAN geometry introduced in (Paganini et al., 2018a). [‡]Reflects the time to generate directly the point cloud representation, which is more granular than the corresponding GEANT4 generation

image representation, each layer $\mathbf{x}_{L_i} = \{E_j^i\}_{j \in \mathcal{G}_i}$ where \mathcal{G}_i represents the discretized and fixed (ordered) grid for i^{th} layer. Further, we denote the bin centers in η direction as \mathcal{H}_i and in ϕ direction as \mathcal{F}_i .

Algorithm 1 SUPA - Particle Splitting

Globals: $p_{stop} = [0.9 * (x/27)^{1.25}$ for $x \in \text{range}(28)]$
 ReadOut : { Layer 0 : (5, ..., 9),
 Layer 1 : (10, ..., 18),
 Layer 2 : (19, ... 28) }
 Layer Depth $\Delta z = 2$

Input: Tree \mathcal{T} , Position $\mathbf{p} = (\Delta\eta, \Delta\phi)$,
 Energy E , Layer l

Output: a collection of $\{\mathbf{p}_i, E_i\}^N$ of generated particles

Parameters: $p_\theta(\cdot) \sim \mathcal{U}(\pi/2, \pi/4)$, $p_\epsilon(\cdot) \sim \mathcal{U}(-\theta/4, \theta/4)$

- 1: $(\mathbf{p}, E, l) \leftarrow \text{Input}, N \leftarrow p(\delta(n=2))$
- 2: $\theta \sim p_\theta(\cdot), \epsilon \sim p_\epsilon(\cdot), \alpha \sim \mathcal{U}(0, 1)$
- 3: **if** $\alpha < p_{stop}[l]$ and $l > 6$ **then**
- 4: Active \leftarrow False
- 5: **else if** $p_{stop}[l] < \alpha < p_{stop}[l] + p_{decay}$ **then**
- 6: **if** $\mathcal{U}(0, 1) < 0.5$ **then**
- 7: $\mathbf{p}_{\{0,1\}} \leftarrow \mathbf{p} + (0, \Delta z * \tan(\theta/2 \{+, -\} \epsilon))$
- 8: **else**
- 9: $\mathbf{p}_{\{0,1\}} \leftarrow \mathbf{p} + (\Delta z * \tan(\theta/2 \{+, -\} \epsilon), 0)$
- 10: **end if**
- 11: $E_{\{0,1\}} \leftarrow E * (\theta/2 \{+, -\} \epsilon) / \theta$
- 12: $\mathcal{T}.add(\mathbf{p}_0, l+1, E_0), \mathcal{T}.add(\mathbf{p}_1, l+1, E_1)$
- 13: **else**
- 14: $\mathcal{T}.add(\mathbf{p}, l+1, E)$
- 15: **end if**
- 16: Return \mathcal{T}

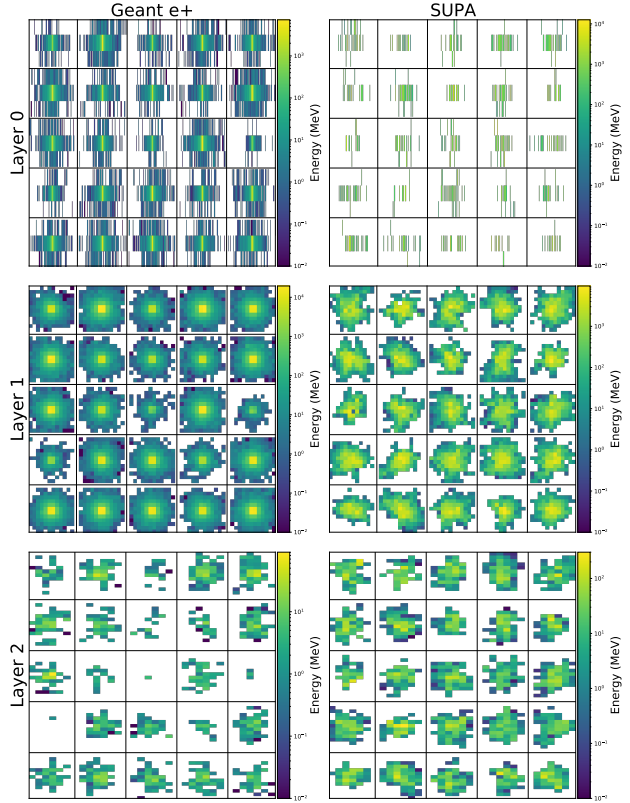


Figure 4: 25 randomly selected e^+ events of GEANT4 (left) and SUPA (right). We do not expect them to match as our goal is not to reproduce the exact distribution. However, we still want to produce data with a rich and complex structure.

4. Evaluation Metrics

The evaluation of generative models for high dimensional data is a non-trivial problem. While reconstruction losses and/or data likelihood are available for some model architectures (e.g. auto-encoders or flows), judging the sample quality is still difficult. Moreover, the average log-likelihood is difficult to evaluate or even approximate for many interesting models. For instance, in computer vision, evaluating generative models for images is done via proxy measures such as the Frchet Inception Distances (FID, Heusel et al., 2017).

Prior works on generative models for calorimetry data (shower simulations) have used histograms of different metrics called *shower shape variables* in addition to images of calorimeter showers to judge the quality of generative models. These shower shape variables are domain specific and physically motivated, and matching densities over these marginals is indicative of matching salient aspects of the data. In this section, we will review these shower shape vari-

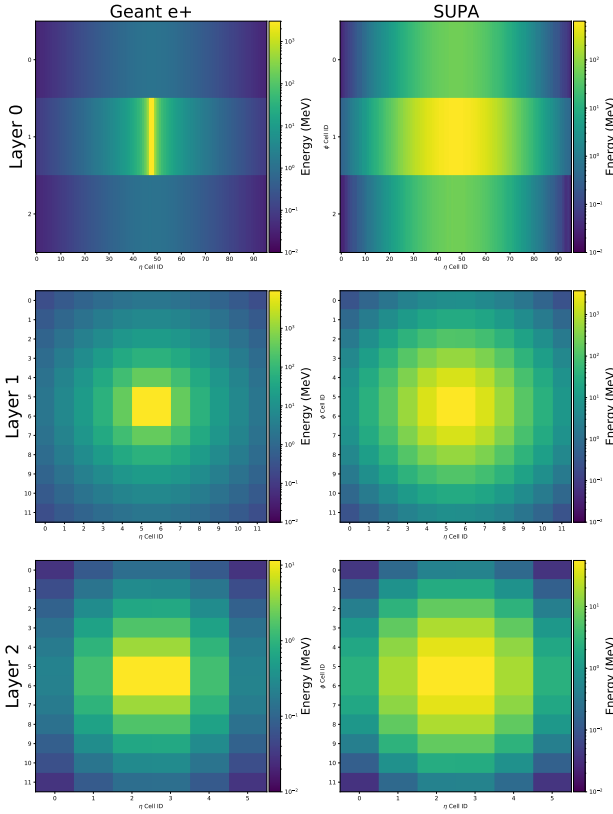


Figure 5: Average shower shapes. Rows are calorimeter layers 0 to 2, left column shows e^+ events from GEANT4 and right column shows events from SUPA

ables, and introduce a few others. Furthermore, we extend many of these metrics for the point cloud representation³ of showers.

In order to summarise the discrepancy into a scalar value, we use the Wasserstein-1 distance between the histograms of the ground truth and generated sample’s marginals. Further, we compute the **mean discrepancy** over all the marginals as a final performance metric for each model.

We consider the following variables:

Layer Energy E_i . Denotes the total energy deposited in layer i of the shower. $E_i = \sum_{j \in \mathcal{G}_i} E_j^i$ or $E_i = \sum_{j \in \mathcal{N}_i} E_j^i$.

Total Energy E_{tot} . Total energy across all layers of the shower. $E_{\text{tot}} = \sum_{i \leq N} E_i$.

Layer Energy Fraction f_i . Fraction of the total energy

³Shower shape variables for the image representation are still valid and interesting to compare when generative models are trained directly on the point cloud representation as we can always obtain the image representation by downsampling the point clouds at different scales

deposited in layer i of the shower. $f_i = E_i/E_{\text{tot}}$.

Cell Energy Ratio $E_{\text{ratio},i}$. Ratio of the difference between highest and second highest energy intensity point or cell in layer i and their difference.

$$E_{\text{ratio},i} = \frac{E_{[1]}^i - E_{[2]}^i}{E_{[1]}^i + E_{[2]}^i}.$$

Depth d . Deepest layer in the shower with non-zero energy deposit. $d = \max_i \{i : \max_j (E_j^i) > 0\}$.

Layer/Depth Weighted Total Energy l_d . Sum of the layer energies weighted by the layer number. $l_d = \sum_{i \leq N} i \cdot E_i$.

Shower Depth s_d . Depth weighted total energy normalized by the total energy in the shower. $s_d = l_d/E_{\text{tot}}$.

Shower Depth Width σ_{s_d} . Standard deviation of s_d in units of layer number.

$$\sigma_{s_d} = \sqrt{\frac{\sum_{i=0}^2 i^2 \cdot E_i}{E_{\text{tot}}} - \left(\frac{\sum_{i=0}^2 i \cdot E_i}{E_{\text{tot}}}\right)^2}$$

Layer Centroids $\langle \eta_i \rangle, \langle \phi_i \rangle$. Mean of grid position (η or ϕ) weighted by the deposited energy.

$$\langle \eta_i \rangle = \frac{\mathbf{x}_{L_i} \odot \mathcal{H}_i}{E_i}, \quad \langle \phi_i \rangle = \frac{\mathbf{x}_{L_i} \odot \mathcal{F}_i}{E_i}$$

Here \odot denotes element-wise multiplication. For point cloud representation, this can be generalized as :

$$\langle \eta_i \rangle = \frac{\sum_j E_j^i \eta_j^i}{E_i}, \quad \langle \phi_i \rangle = \frac{\sum_j E_j^i \phi_j^i}{E_i}$$

Layer Lateral Width σ_i . Denotes the standard deviation of the η centroid.

$$\sigma_i = \sqrt{\frac{\mathbf{x}_{L_i} \odot \mathcal{H}_i^2}{E_i} - \left(\frac{\mathbf{x}_{L_i} \odot \mathcal{H}_i}{E_i}\right)^2}$$

Brightest Voxels $E_{k_brightest_layer_i}$. The k^{th} brightest voxel in layer i normalized by the total layer energy. $E_{k_brightest_layer_i} = E_{[k]}^i/E_i$.

Layer Sparsity. The ratio of the number of cells with non-zero energy to the total number of cells in layer i . This is only valid for the image representation of showers.

5. Experiments

5.1. Validity of SUPA as a benchmark

We train the models of § 2.2 on both the events generated by GEANT4 and SUPA. The training loss of the flow model is a

log-likelihood which meaningfully represents the quality of the captured distribution. Figure 6 displays the correlation of the log-likelihood values of different variations of the CaloFlow architecture trained both on GEANT4 and SUPA-generated events. Figure 7 shows the scatter plot of the mean discrepancy (see § 5.1) obtained by different models on GEANT4 and SUPA-generated events, while Figure 8 shows the scatter plot of the average ranks of those models. The average rank for a model on a dataset is obtained by first ranking them with respect to each marginal’s discrepancy and then averaging over all the marginals. We can observe that all these correlation plots are roughly monotonic, showing that benchmarking on SUPA provides a good estimate of relative performance on the detailed GEANT4.

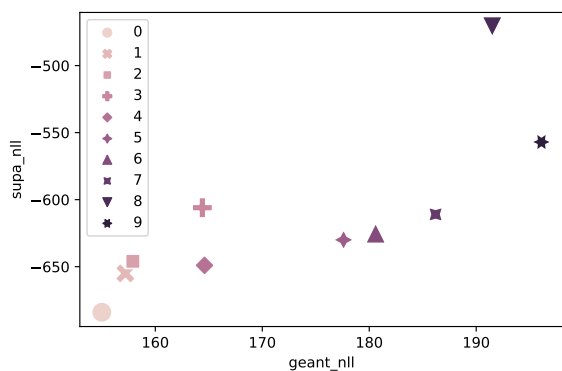


Figure 6: Scatter Plot for the loss over 10 different versions of CaloFlow models. Each point corresponds to an architecture, its x and y coordinates are the negative log-likelihoods on data generated by GEANT4 and SUPA, respectively. Increasing label numbers denote models with decreasing capacity (number of layers, learnable parameters, etc.).

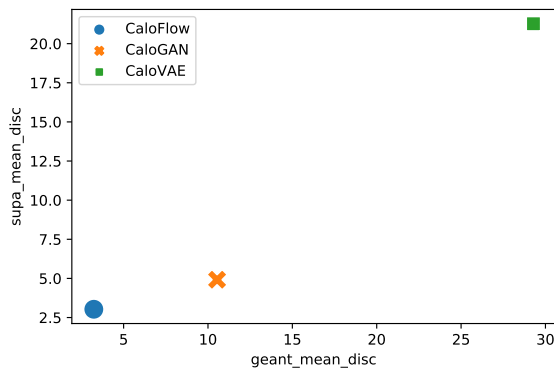


Figure 7: Scatter Plot for mean discrepancy (§ 4) over different models. Lower numbers are better. Performance of models are consistent over both datasets, a better model on SUPA implies a better model on GEANT4 and vice versa.

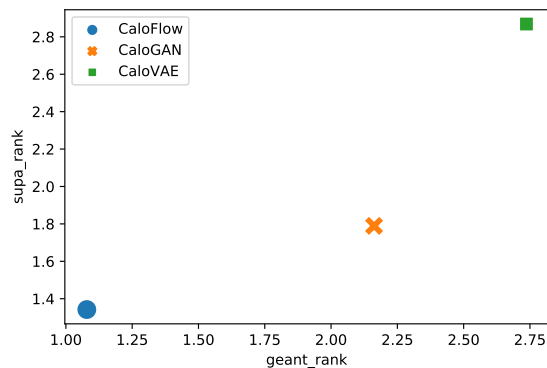


Figure 8: Scatter Plot for ranks over different models. Ranking of the models are consistent over both, SUPA and GEANT4, showing the validity of SUPA as a benchmark.

Further, in Figure 9, (and Figures 10, 11, 12, 13, 14 in the Appendix) we show a subset of the marginals (see § 4 for a detailed explanation on the marginals) for GEANT4 and SUPA and also the showers generated with different models trained on them. These marginal plots illustrate the diversity in various distributions present in data from GEANT4, and, more importantly in SUPA. Further, the distributions of the generated showers from different models behave similarly on both datasets, reinstating the proposition that a better model on SUPA implies a better model on the detailed GEANT4.

Table 2: Mean discrepancy metric (see § 5.1) for CaloFlow model when trained and tested over different resolutions. Columns correspond to the training resolution and rows to the test resolution. The results on the diagonal show that CaloFlow’s performance degrades when resolution increases, and the top row shows that it is not simply due to the sheer dimensionality of the signal since the model does not leverage structure at high resolution to perform better at low resolution.

	1x	2x	3x
1x	3.57	6.35	7.20
2x	-	6.78	-
3x	-	-	8.29

5.2. High-resolution experiments

In this section, we show the utility of SUPA beyond using it for training at low resolution (similar to the resolution used in CaloGAN, which we call 1x), as well as the limitation of the current models.

We train CaloFlow (Krause & Shih, 2021) with SUPA by downsampling the point clouds at the higher resolutions of

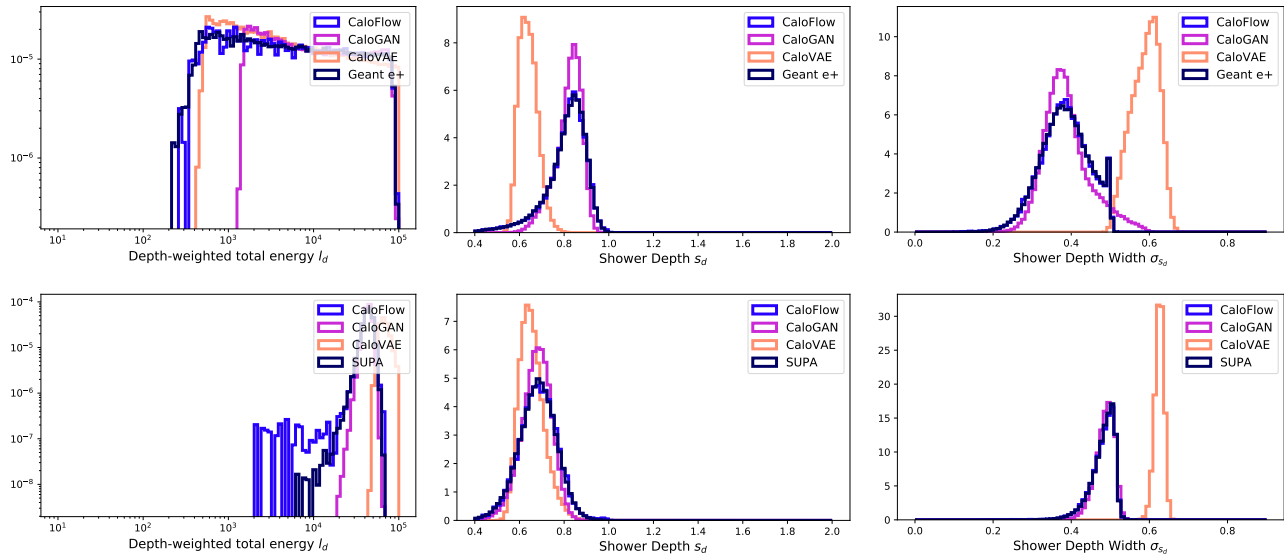


Figure 9: Histogram for various marginals for GEANT4 e+ (top) and SUPA (bottom) vs. showers generated from different trained models

2x and 3x. Table 2 shows the mean discrepancy metric (see § 5.1) for the models. We observe the trend that training at higher resolutions result in poorer performance (diagonal terms) in general. Further, when the generated samples from the trained models are downsampled to 1x, the performance deteriorates as compared to samples generated from models trained directly with data at 1x resolution.

6. Conclusion

We introduced SUPA, a lightweight pseudo-particle simulator that is inspired by the physics governed development of particle showers and qualitatively resembles the data generated by the gold standard GEANT4. We showed in § 5.1 that performance of deep generative models estimated on data produced with this simulator is a good proxy for their performance on the standard data used historically in machine learning for particle physics.

We believe that the ease of use, flexibility and speed of this simulator could be a MNIST moment for the field, allowing the rapid exploration of models in various regime of functioning, such as higher resolutions as illustrated in § 5.2.

By allowing to easily change the underlying parameters of the propagation model, we introduce the freedom to define new benchmark datasets of varying complexity with a fidelity and simplicity not available using the GEANT4 toolkit.

Additionally, by giving easy access to the fully recorded event, we open the way to applying methods from point

clouds and geometric deep learning research, with the goal of possibly devising end-to-end architecture able to reconstruct a full event from the energy deposits by solving the complete inverse problem, something currently impossible with data from GEANT4. The code for SUPA is available under MIT license at <https://github.com/itsdaniele/SUPA>.

7. Disclosure of Funding

The authors would like to acknowledge funding through the SNSF Sinergia grant called Robust Deep Density Models for High-Energy Particle Physics and Solar Flare Analysis (RODEM) with funding number CRSII5_193716.

References

- Abhishek, A., Drechsler, E., Fedorko, W., and Stelzer, B. Calodvae: Discrete variational autoencoders for fast calorimeter shower simulation. 2021.
- Agostinelli, S., Allison, J., Amako, K., Apostolakis, J., Araujo, H., Arce, P., Asai, M., Axen, D., Banerjee, S., Barrand, G., Behner, F., Bellagamba, L., Boudreau, J., Broglia, L., Brunengo, A., Burkhardt, H., Chauvie, S., Chuma, J., Chytrcek, R., Cooperman, G., Cosmo, G., Degtyarenko, P., Dell’Acqua, A., Depaola, G., Dietrich, D., Enami, R., Feliciello, A., Ferguson, C., Fesefeldt, H., Folger, G., Foppiano, F., Forti, A., Garelli, S., Giani, S., Giannitrapani, R., Gibin, D., Gómez Cadenas, J., González, I., Gracia Abril, G., Greeniaus, G., Greiner, W., Grichine, V., Grossheim, A., Guatelli, S., Gumplinger, P., Hamatsu, R., Hashimoto, K., Hasui, H., Heikkinen,

- A., Howard, A., Ivanchenko, V., Johnson, A., Jones, F., Kallenbach, J., Kanaya, N., Kawabata, M., Kawabata, Y., Kawaguti, M., Kelner, S., Kent, P., Kimura, A., Kodama, T., Kokoulin, R., Kossov, M., Kurashige, H., Lamanna, E., Lampén, T., Lara, V., Lefebure, V., Lei, F., Liendl, M., Lockman, W., Longo, F., Magni, S., Maire, M., Medernach, E., Minamimoto, K., Mora de Freitas, P., Morita, Y., Murakami, K., Nagamatu, M., Nartallo, R., Nieminen, P., Nishimura, T., Ohtsubo, K., Okamura, M., O’Neale, S., Oohata, Y., Paech, K., Perl, J., Pfeiffer, A., Pia, M., Ranjard, F., Rybin, A., Sadilov, S., Di Salvo, E., Santin, G., Sasaki, T., Savvas, N., Sawada, Y., Scherer, S., Sei, S., Sirotenko, V., Smith, D., Starkov, N., Stoecker, H., Sulkimo, J., Takahata, M., Tanaka, S., Tcherniaev, E., Safai Tehrani, E., Tropeano, M., Truscott, P., Uno, H., Urban, L., Urban, P., Verderi, M., Walkden, A., Wander, W., Weber, H., Wellisch, J., Wenaus, T., Williams, D., Wright, D., Yamada, T., Yoshida, H., and Zschesche, D. Geant4—a simulation toolkit. *Nuclear Instruments and Methods in Physics Research Section A: Accelerators, Spectrometers, Detectors and Associated Equipment*, 506(3):250–303, 2003. ISSN 0168-9002. doi: [https://doi.org/10.1016/S0168-9002\(03\)01368-8](https://doi.org/10.1016/S0168-9002(03)01368-8). URL <https://www.sciencedirect.com/science/article/pii/S0168900203013688>.
- ATLAS collaboration. Deep generative models for fast shower simulation in atlas. <http://cdsweb.cern.ch/record/2630433/files/ATL-SOFT-PUB-2018-001.pdf>, 2018. Accessed: 2022-01-26.
- Belayneh, D., Carminati, F., Farbin, A., Hooberman, B., Khattak, G., Liu, M., Liu, J., Olivito, D., Pacela, V. B., Pierini, M., et al. Calorimetry with deep learning: particle simulation and reconstruction for collider physics. *The European Physical Journal C*, 80(7):1–31, 2020.
- Buhmann, E., Diefenbacher, S., Eren, E., Gaede, F., Kasieczka, G., Korol, A., and Krüger, K. Decoding photons: Physics in the latent space of a bib-ae generative network. *arXiv preprint arXiv:2102.12491*, 2021a.
- Buhmann, E., Diefenbacher, S., Eren, E., Gaede, F., Kasieczka, G., Korol, A., and Krüger, K. Getting high: high fidelity simulation of high granularity calorimeters with high speed. *Computing and Software for Big Science*, 5(1):1–17, 2021b.
- Chang, A. X., Funkhouser, T., Guibas, L., Hanrahan, P., Huang, Q., Li, Z., Savarese, S., Savva, M., Song, S., Su, H., Xiao, J., Yi, L., and Yu, F. ShapeNet: An Information-Rich 3D Model Repository. Technical Report arXiv:1512.03012 [cs.GR], Stanford University — Princeton University — Toyota Technological Institute at Chicago, 2015.
- de Oliveira, L., Paganini, M., and Nachman, B. Learning particle physics by example: Location-aware generative adversarial networks for physics synthesis. *Computing and Software for Big Science*, 1(1), Sep 2017. ISSN 2510-2044. doi: 10.1007/s41781-017-0004-6. URL <http://dx.doi.org/10.1007/s41781-017-0004-6>.
- Erdmann, M., Geiger, L., Glombitza, J., and Schmidt, D. Generating and refining particle detector simulations using the wasserstein distance in adversarial networks. *Computing and Software for Big Science*, 2(1):1–9, 2018.
- Erdmann, M., Glombitza, J., and Quast, T. Precise simulation of electromagnetic calorimeter showers using a wasserstein generative adversarial network. *Computing and Software for Big Science*, 3(1):1–13, 2019.
- Goodfellow, I., Pouget-Abadie, J., Mirza, M., Xu, B., Warde-Farley, D., Ozair, S., Courville, A., and Bengio, Y. Generative adversarial nets. In Ghahramani, Z., Welling, M., Cortes, C., Lawrence, N., and Weinberger, K. Q. (eds.), *Advances in Neural Information Processing Systems*, volume 27. Curran Associates, Inc., 2014. URL <https://proceedings.neurips.cc/paper/2014/file/5ca3e9b122f61f8f06494c97b1afccf3-Paper.pdf>.
- Heusel, M., Ramsauer, H., Unterthiner, T., Nessler, B., and Hochreiter, S. GANs trained by a two time-scale update rule converge to a local Nash equilibrium. In *Advances in Neural Information Processing Systems*, 2017.
- Kingma, D. P. and Welling, M. Auto-encoding variational bayes, 2014.
- Krause, C. and Shih, D. Caloflow: Fast and accurate generation of calorimeter showers with normalizing flows, 2021.
- Paganini, M., de Oliveira, L., and Nachman, B. Calogan: Simulating 3d high energy particle showers in multilayer electromagnetic calorimeters with generative adversarial networks. *Physical Review D*, 97(1), Jan 2018a. ISSN 2470-0029. doi: 10.1103/physrevd.97.014021. URL <http://dx.doi.org/10.1103/PhysRevD.97.014021>.
- Paganini, M., de Oliveira, L., and Nachman, B. Calogan: Simulating 3d high energy particle showers in multilayer electromagnetic calorimeters with generative adversarial networks. *Physical Review D*, 97(1):014021, 2018b.
- Radford, A., Metz, L., and Chintala, S. Unsupervised representation learning with deep convolutional generative adversarial networks, 2016.

Rezende, D. J. and Mohamed, S. Variational inference with normalizing flows, 2016.

Wu, Z., Song, S., Khosla, A., Yu, F., Zhang, L., Tang, X., and Xiao, J. 3d shapenets: A deep representation for volumetric shapes, 2015.

A. Histograms for Shower Shape Variables

We show some of the remaining marginals for GEANT4 and SUPA and also for the showers generated with different models trained on them.

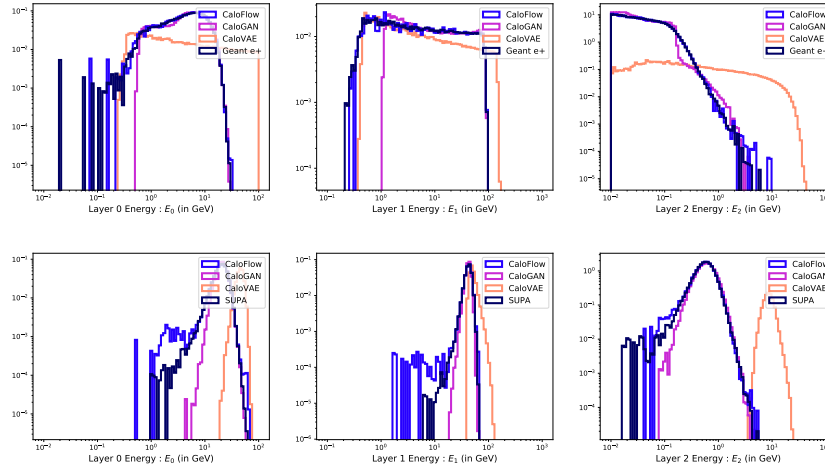


Figure 10: Histogram for Layer Energy for GEANT4 e+ (top) and SUPA (bottom) vs. showers generated with different trained models.

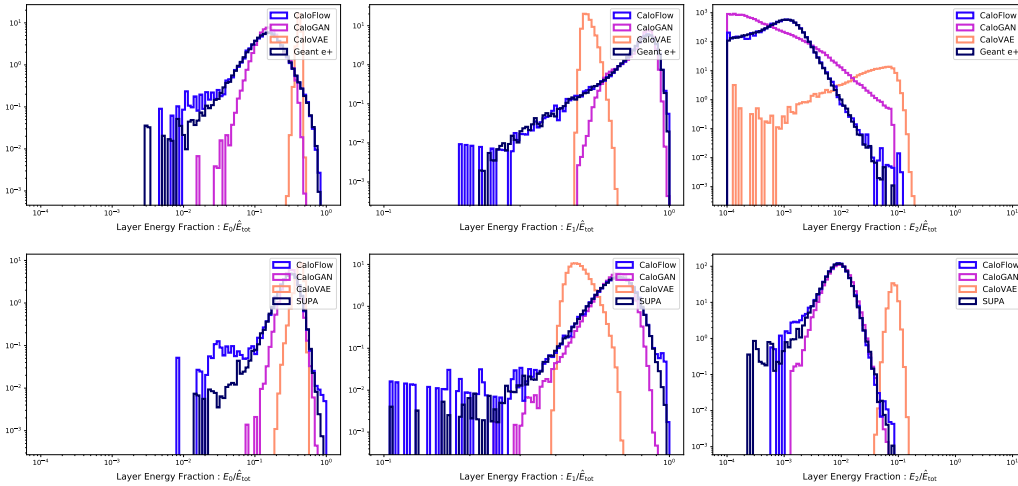


Figure 11: Histogram for Layer energy fraction for GEANT4 e+ (top) and SUPA (bottom) vs. showers generated with different trained models.

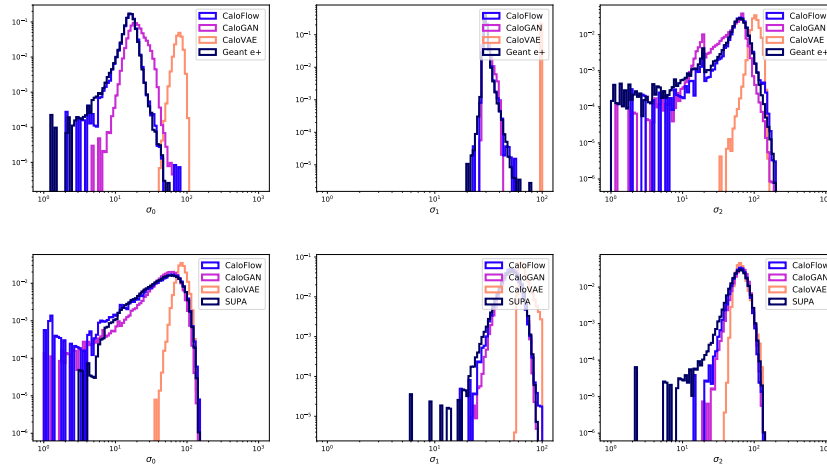


Figure 12: Histogram for Layer lateral width for GEANT4 e+ (top) and SUPA (bottom) vs. showers generated with different trained models.

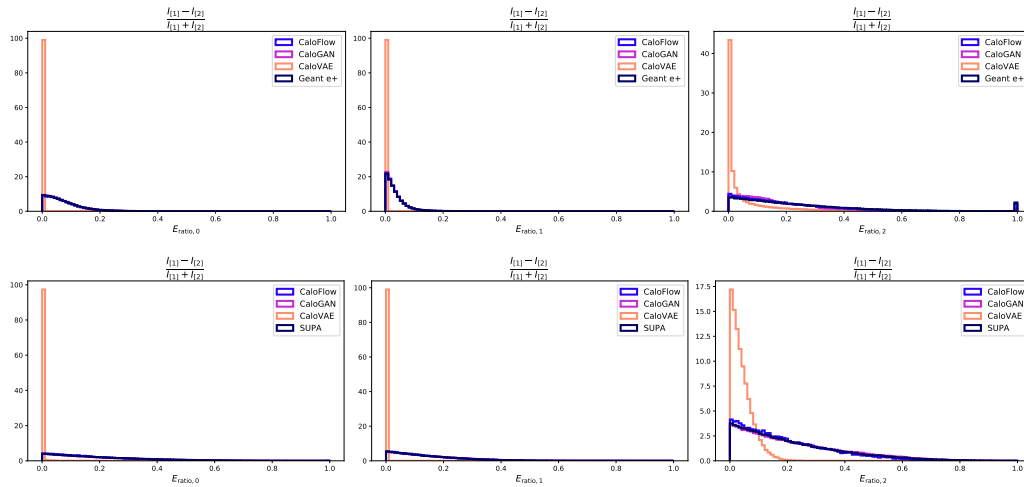


Figure 13: Histogram for $E_{ratio,i}$ for GEANT4 e+ (top) and SUPA (bottom) vs. showers generated with different trained models.

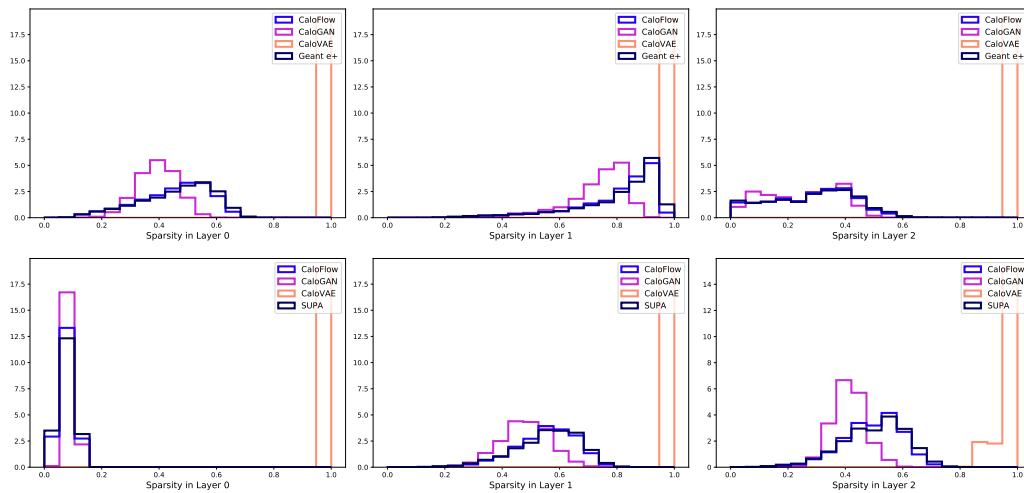


Figure 14: Histogram for Layer sparsity for GEANT4 e+ (top) and SUPA (bottom) vs. showers generated with different trained models.